Simulation-Based Engineering Lab
University of Wisconsin-Madison

Technical Report TR-2016-16

Using the Complementarity and Penalty Methods for Solving Frictional Contact Problems in Chrono: Validation for the Cone Penetration Test

Michał Kwarta and Dan Negrut

Version: March 24, 2017

Abstract

The numerical results of cone penetration test were presented and validated against experimental ones. Two different approaches for modeling the dynamics of granular matter were used. The first one, discrete element method with penalty contact modeling (DEM-P) [1], is an approach usually used in e. g. granular flows or powder mechanics simulations. The second method, called DEM-C (from "complementarity") is essential in fields like robotics and graphics [2]. In this approach the bodies cannot penetrate due to the complementarity conditions. Even though the methods model contact with friction in two different ways, as well as they can be described by using two very different sets of mechanical and numerical parameters, the results obtained from the simulations were comparable. The validation study was enriched by the performance analysis. We also examined how sensitive the simulations were to the changes of certain parameters' values and particles shape. To obtain the results, an open source software package, called Chrono was used [3]. The source code of the model used in the numerical experiments is available on-line.

Keywords: cone penetration test, penalty contact modeling, differential variational inequality modeling, friction, contact

Contents

Nomenclature

Abbreviations

DEM-P	Discrete Element Method - Penalty
DEM-C	Discrete Element Method - Complementarity
CPT	Cone Penetrometer Test
LVDT	Linear Variable Differential Transformer

Mathematical notation

$\mathrm{N}(\mu,\, \sigma^2)$	Normal distribution with mean μ and variance σ^2

Physical parameters

Y	Young's modulus
ν	Poisson's ratio
ϱ	density
g	Earth's gravity
a	average value of the upward acceleration caused by the friction force between the LVDT apparatus' rod and its track, $a = 2.21 \frac{m}{s^2}$
μ_{p-p}	inter-sphere coefficient of friction
μ_{p-w}	coefficient of friction between particles and container's walls
μ_{p-c}	coefficient of friction between particles and cones
$c_{r,p-p}$	inter-sphere coefficient of restitution
$c_{r,p-w}$	coefficient of restitution between particles and container's walls
$c_{r,p-c}$	coefficient of restitution between particles and cones
L_{30°	height of the cone with 30° in apex angle, $\mathrm{L}_{30^\circ} = 34.36$ mm
W_{30°	width of the base's diameter of the cone with 30° in apex angle, $\mathrm{W}_{30^\circ} = 9.21$ mm
L_{60°	height of the cone with 60° in apex angle, $\mathrm{L}_{60^\circ} = 22.10$ mm
W_{60°	width of the base's diameter of the cone with 60° in apex angle, $\mathrm{W}_{60^\circ} = 19.86$ mm
H	height (relative to the granular material surface) the cones were dropped from; $\mathrm{H} \in \{0,\ \frac{1}{2}\mathrm{L_i},\ \mathrm{L_i}\}$, $\mathrm{i} \in \{30^\circ,\ 60^\circ\}$

Numerical parameters

Δt	time step
MNoI	maximum number of iterations
CRS	contact recovery speed

1 Laboratory Experiments

1.1 Overview

The detailed report concerning the laboratory cone penetration test can be found in [4]. In this section aspects of the experiment which needed to be considered during the numerical modeling were described. The mechanical and geometrical parameters of the bodies used in the empirical tests were provided. The impact of the experimental apparatus on the results was briefly described as well.

The laboratory tests were conducted on using two cylindrical containers with diameters equal to 4 and 6 in (10.16 and 15.24 cm respectively). They were 11.64-cm-high and fully filled out with a specimen made of imperfect spheres (see Table 1). Those imperfect spheres were made of glass and could be modeled as ellipsoids of diameters from the following normal distribution: N(2.84, 0.0834) mm (Table 2).

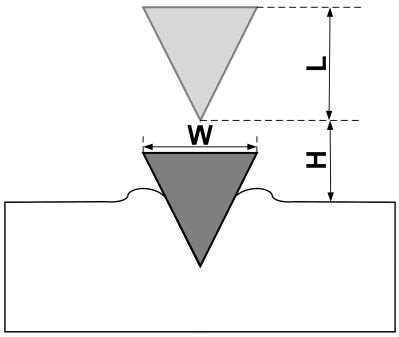

Figure 1: Schematic diagram of a cone drop experiment. The drop height (H), cone height (L) and width (W) are illustrated in the picture.

	Diameter [in (cm)]	Height [cm]
Containers	4 (10.16) 6 (15.24)	11.64

Table 1: Geometrical dimensions of the **containers** used in the experiments

Following the standardized procedures (ASTM D5254) specimens used in the experiments were placed in containers in the ways that allow them having two different densities and void ratios (Table 3).

Cones of two different geometrical dimensions were dropped on such prepared granular materials. In the first scenario the cone had height $L_{30^\circ} = 34.36$ mm, the base's diameter $W_{30^\circ} = 9.21$ mm and the apex angle equal to 30°. The other cone was 22.10-mm-high (L_{60°), the diameter of its base (W_{60°) was 19.86-mm-wide and it had the apex angle of 60°. The cones were made of brass steel of following mechanical parameters: Young's modulus $193 \cdot 10^9$ Pa and Poisson's ratio between $0.3 \div 0.31$ (Table 4).

(a) Cone (with 30° in the apex angle) attached to the LVDT connector. The rod putting a kinematic constraint on the cone's motion and rod's track can also be seen in this picture.

(b) One of the containers used in the experiment filled out with the granular material. The measuring apparatus is placed above it. Picture was taken right before one of the tests was conducted on.

Figure 2: Pictures of the apparatus used in the experiment.

The cone was attached, with a special connector, to a Linear Variable Differential Transformer (LVDT) - the apparatus which monitored the cone's vertical position while it was falling and penetrating the granular media. The mass of the cones, 30° and 60° in apex angle, together with the LVDT connector was equal to 141.1 g and 135.7 g, respectively (Table 4).

Besides attaching an additional mass to the falling bodies, the LVDT apparatus affected the experimental results in two more ways. Firstly, it put a kinematic constraint on the cone's trajectory. Namely, the cone's axis of symmetry had to remain vertical at the every time instant of it's motion. It was caused by the fact of using the vertical rod connecting the cone with the rest of the machinery (Figure 2a). Secondly, there was a friction force acting between the before-mentioned rod and its track. The value of the force was measured during all the experiments conducted on. Its average value was calculated, receiving 0.03 N, what decreased the cones' downward acceleration by 2.21 $\frac{\mathrm{m}}{\mathrm{s}^2}$.

	Shape	Diameters distribution [mm]	Material
Granular material	Ellipsoids	N(2.84, 0.0834)	Glass

Table 2: Geometrical dimensions and material of the **particles** used in the experiments

The last information that had to taken into account while setting up the simulations was the height (relative to the surface of the settled specimen) from which the cones were

(a) Cones with 60° and 30° in the apex angle.

(b) Cones with LVDT connectors attached.

Figure 3: Pictures of the cones used in the experiment.

dropped. In the static cone penetration test, the cone was placed on the surface of the granular material at zero drop height. In the dynamic loading, the cone was dropped at several heights above the surface of the granular material. The laboratory test of the dynamic loading was conducted for two different initial heights of cones. First one, was equal to the dropped cone's height ($L_{30^\circ} = 34.36$ mm, $L_{60^\circ} = 22.10$ mm), and the other one equal to the half of its height ($\frac{1}{2}L_{30^\circ} = 17.18$ mm, $\frac{1}{2}L_{60^\circ} = 11.05$ mm).

	Density $\left[\frac{\text{kg}}{\text{m}^3}\right]$	Void Ratio
Loose Case	1504.32	0.66
Dense Case	1630.35	0.53

Table 3: Densities and void ratios of specimens used in the empirical tests

	Apex angle	Height [mm]	Base's Diameter [mm]	Y [Pa]	ν	mass* [g]
Cones	30°	34.36	9.21	$193 \cdot 10^9$	$0.3 \div 0.31$	141.1
	60°	22.10	19.86			135.7

Table 4: Geometrical dimensions and mechanical parameters of the **cones** used in the experiments

* mass of the cones together with the LVDT connector

1.2 Results

Below, the experimental results presented in [4] were showed.

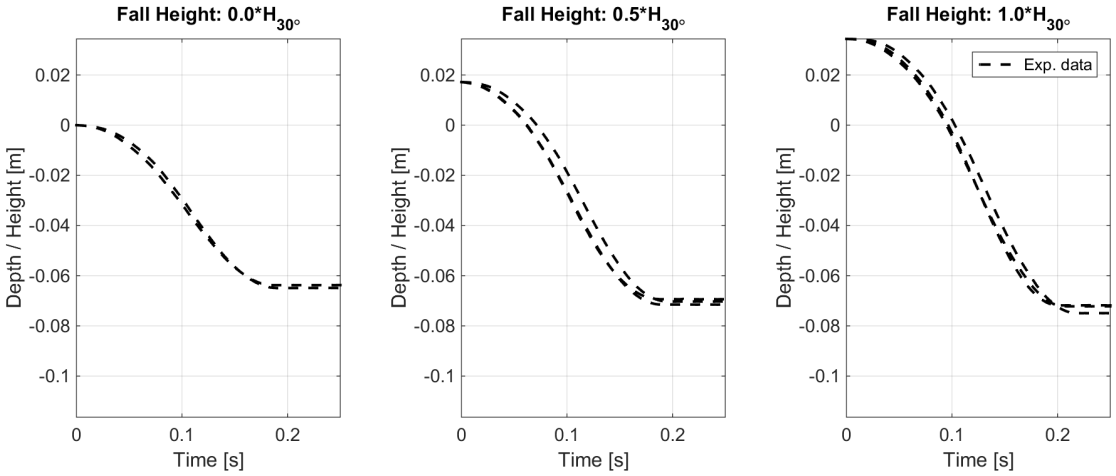

Figure 4: Depth/height vs. time plots of the cone **30°** in apex angle. Container with a **4-inches**-wide diameter. Granular material packed **loosely**.

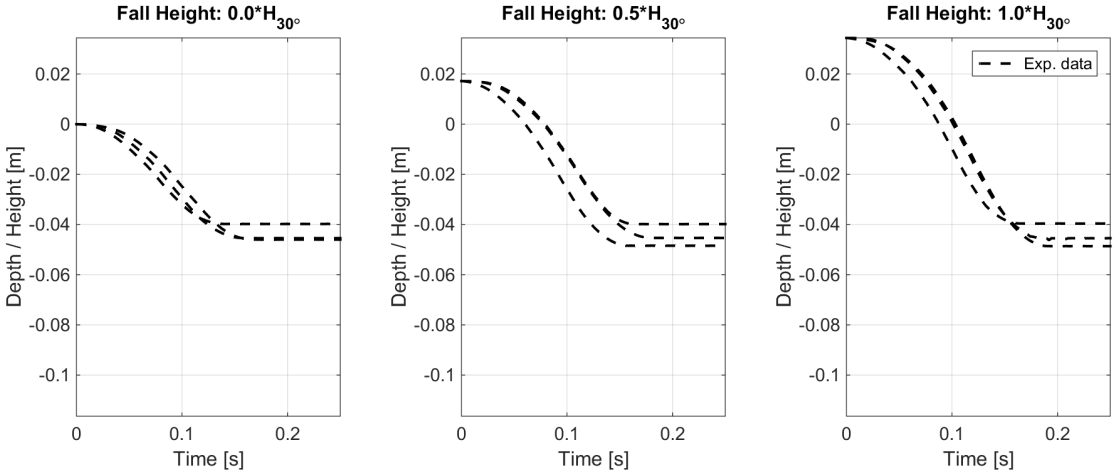

Figure 5: Depth/height vs. time plots of the cone **30°** in apex angle. Container with a **4-inches**-wide diameter. Granular material packed **densely**.

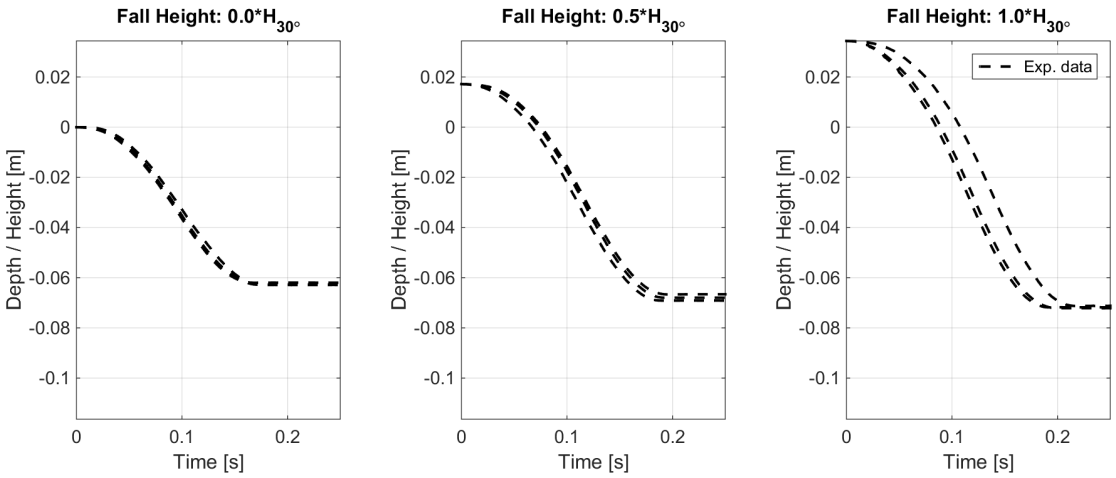

Figure 6: Depth/height vs. time plots of the cone **30**° in apex angle. Container with a **6-inches**-wide diameter. Granular material packed **loosely**.

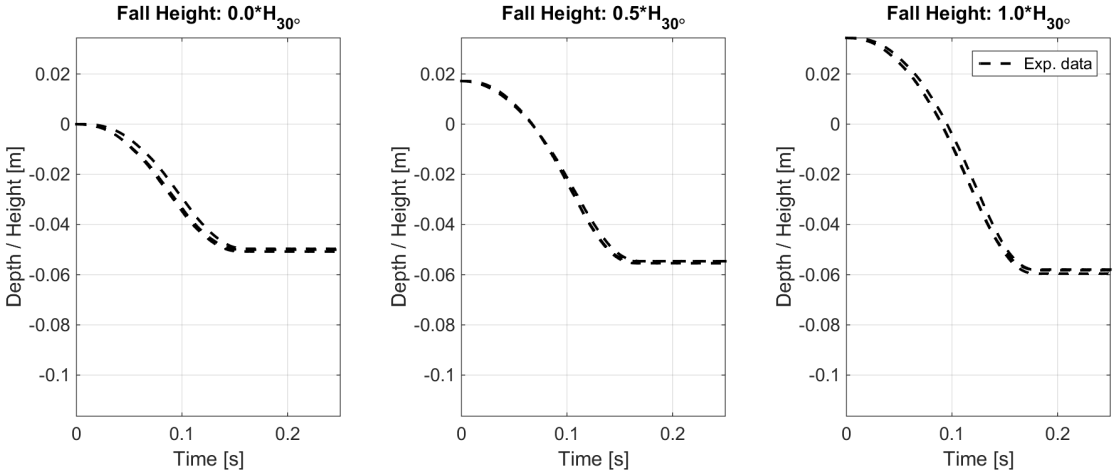

Figure 7: Depth/height vs. time plots of the cone **30**° in apex angle. Container with a **6-inches**-wide diameter. Granular material packed **densely**.

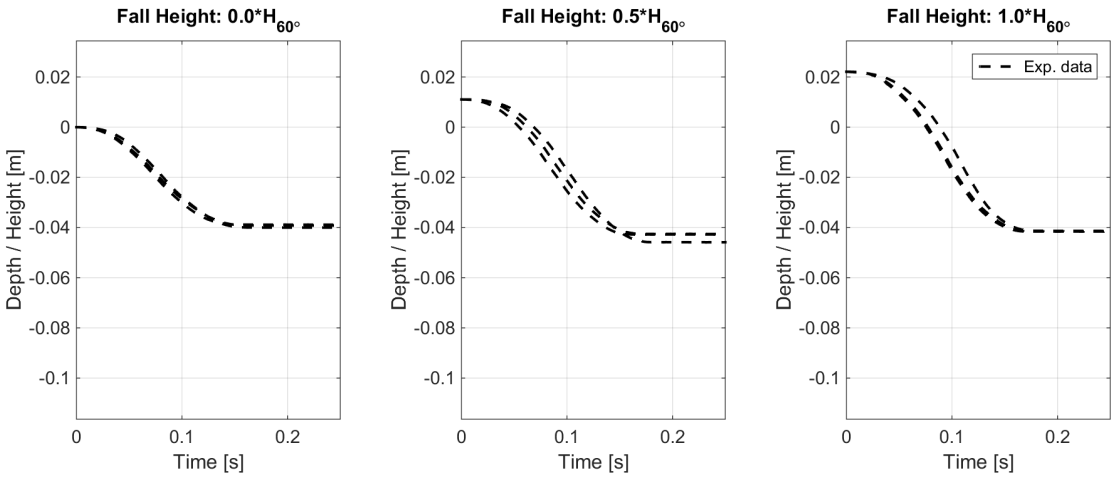

Figure 8: Depth/height vs. time plots of the cone **60**° in apex angle. Container with a **4-inches**-wide diameter. Granular material packed **loosely**.

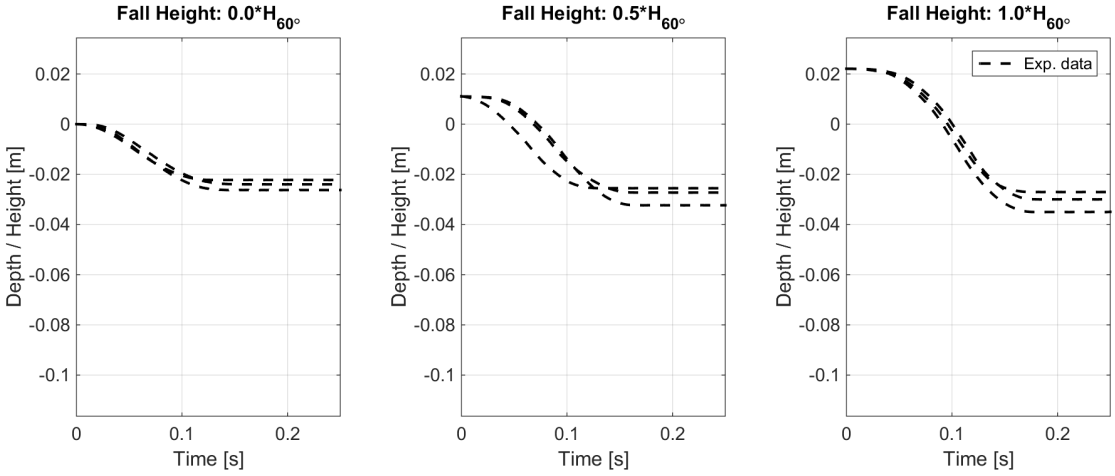

Figure 9: Depth/height vs. time plots of the cone **60**° in apex angle. Container with a **4-inches**-wide diameter. Granular material packed **densely**.

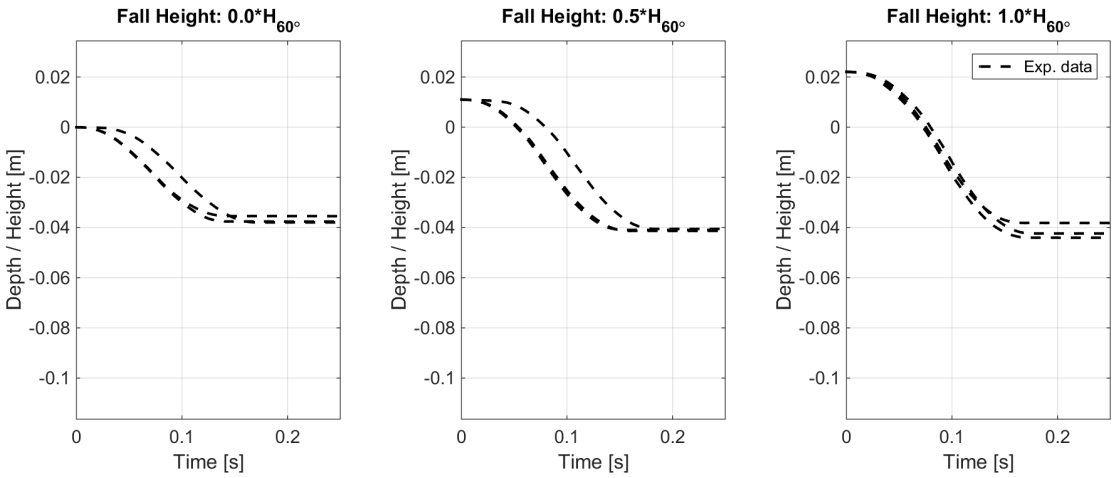

Figure 10: Depth/height vs. time plots of the cone **60**° in apex angle. Container with a **6-inches**-wide diameter. Granular material packed **loosely**.

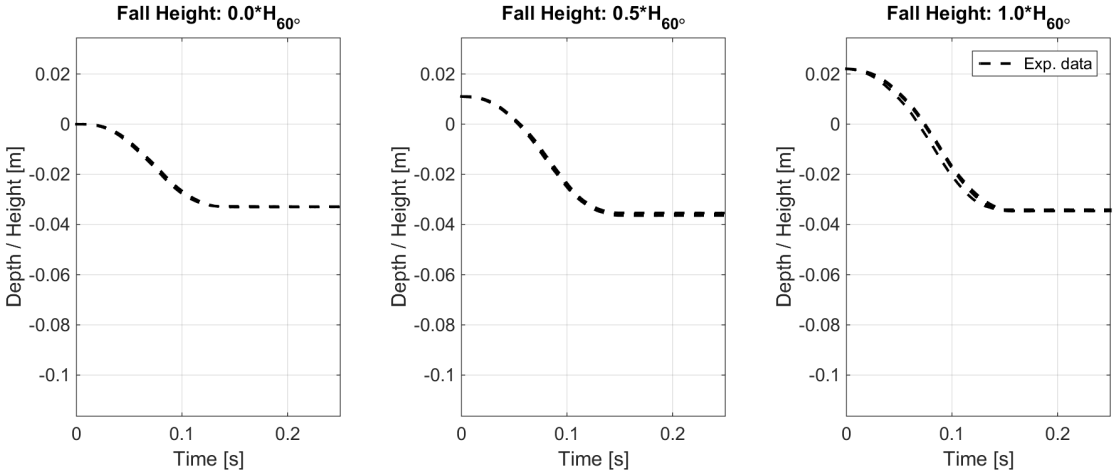

Figure 11: Depth/height vs. time plots of the cone **60**° in apex angle. Container with a **6-inches**-wide diameter. Granular material packed **densely**.

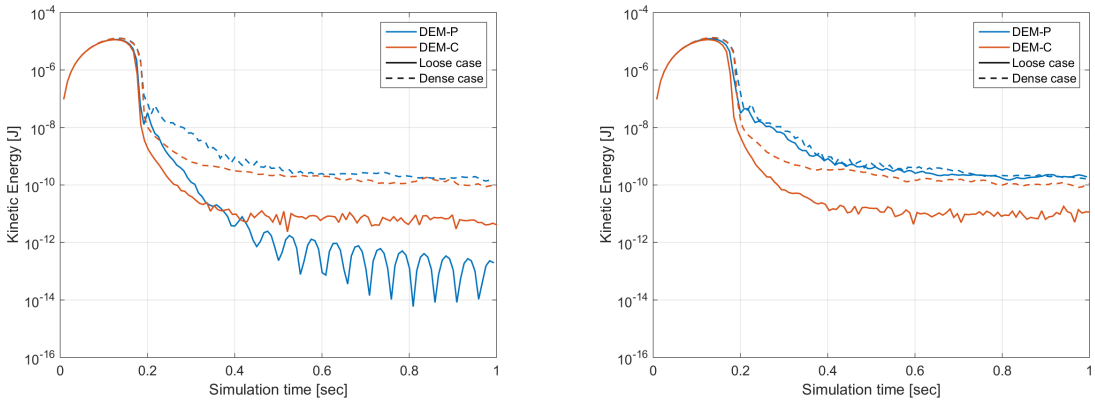

(a) (b)

Figure 12: Kinetic energy of the mechanical system during the settling stage. Simulation with container of diameter equal to (a) 4 inches (b) 6 inches.

2 Numerical Simulations

2.1 Physical Side of the Simulations

The simulations could be divided into two stages. In the first one (settling stage) the specimen was poured into the container and was allowed to gain its equilibrium state (Fig. 12). The second one (cone penetration stage) was about placing the cone right above the surface of the granular material and dropping it with an initial vertical velocity equal to $\sqrt{2(\mathrm{g\text{-}a})\mathrm{H}}$, where:

g was a gravity of Earth,

a was the average upward acceleration caused by the friction force between the LVDT apparatus' rod and its track, $a = 2.21\frac{m}{s^2}$ and

H was one of the three initial heights the cone was dropped from ($\mathrm{H} \in \{0,\ \frac{1}{2}\mathrm{L_i},\ \mathrm{L_i}\}$, $\mathrm{i} \in \{30°,\ 60°\}$)

The containers of a diameter equal to 4 and 6 inches were filled out with the granular material consisted of the perfect spheres. The particles, with diameter of 2.84 mm each, were made of glass of the following mechanical parameters: density 2500 $\frac{\mathrm{kg}}{\mathrm{m}^3}$, Young's modulus 10^8 Pa (value lower than in reality for stability reasons) and Poisson's Ratio 0.3. The coefficient of restitution between particles was set to 0.658 [5]. The walls of the container were massless and had the mechanical parameters of the same values.

A few words of explanation are in order concerning the values of the friction coefficient between particles ($\mu_{\text{particle-particle}}, \mu_{\text{p-p}}$) and between particles and containers' walls ($\mu_{\text{particle-wall}}, \mu_{\text{p-w}}$). Values of those parameters played significant role in obtaining loser and denser packings of the settled specimen. Namely, when the coefficients of friction were set

	Material	$\varrho\left[\frac{\text{kg}}{\text{m}^3}\right]$	Y [Pa]	ν
Granular material	Glass	2500	10^8	0.3

Table 5: The values of **particles**' mechanical parameters used in the simulations

to 0.7 the settled granular material had a density similar to the one obtained in the loose case of the empirical test. The packing seen in the dense case scenario was achieved after the settling simulation with the frictionless particles and walls. In the second part of the simulation (cone penetration test) the before-mentioned friction coefficients together with $\mu_{\text{particle-cone}}$ ($\mu_{\text{p-c}}$) were set to 0.7. The analysis of friction coefficient impact on the results was described in Sections 3.1 and 3.2. The values of friction coefficients for objects made from steel of glass were summarized in [6].

	Material	Apex angle	Y [Pa]	ν	mass* [g]
Cones	Brass Steel	30°	$193 \cdot 10^9$	0.3	141.1
		60°			135.7

Table 6: The values of **cones**' mechanical parameters used in the simulations

Cones used in the simulations were given the geometrical dimensions and mass presented in the Table 4. They were made of brass steel and were given the following parameters: Young's modulus $193 \cdot 10^9$ Pa, Poisson's ratio 0.3. The coefficient of restitution and coefficient of friction between the steel cone an glass beads were equal to: 0.597 [5] and 0.7 [6], respectively.

A kinematic constraint was put on the cone to model the impact of the rod it was attached to. With such constraint cone's symmetry axis remained vertical at the every time instant.

Settling	μ_{p-p}	μ_{p-w}	$c_{r,p-p}$	$c_{r,p-w}$
Loose Case	0.7	0.7	0.658	0.658
Dense Case	0.0	0.0		

CPT Test	μ_{p-p}	μ_{p-w}	$c_{r,p-p}$	$c_{r,p-w}$	μ_{p-c}	$c_{r,p-c}$
Both Cases	0.7	0.7	0.658	0.658	0.7	0.597

Table 7: The values of mechanical parameters describing **contacts** used in the simulations

Approach	time step [s]	MNoI*	CRS** $[\frac{\mathrm{m}}{\mathrm{s}}]$
DEM-P	10^{-5}	-	-
DEM-C	10^{-4}	50	1.0

Table 8: Numerical parameters' values used in the simulations
* MNoI - maximum number of iterations
** CRS - contact recovery speed

2.2 Numerical Side of the Simulations

To simulate the cone penetration test the mechanical system was modeled using two different methods of handling the friction and contact forces between colliding bodies: penalty (DEM-P) and complementarity (DEM-C) method. Those approaches can be successfully used in simulating the mechanical phenomena. If calibrated correctly, simulations based on DEM-P, as well as on DEM-C should give the results that are close enough to empirical measurements and also to each other. Correct calibration is equal to choosing the numerical values for the parameters the two approaches can be characterized with from the numerical point of view. Those values should provide stability of the computations and model the physics sufficiently well.

Stability of calculations in DEM-P model can be ensured by choosing the correct values of the time step (Δt). While using DEM-C method the combination of the following parameters: time step, contact recovery speed (CRS) and maximum number of iterations (MNoI) is important.

In both modeling approaches Δt is the parameter responsible for the stability of calculations. Too large value of the time step will make the simulations unstable, too small - will result in having very long execution time. The optimal value of Δt can be chosen using trial and error method. When it comes to the simulations run so far, the values of the time step used in the simulations based on the DEM-C usually were about 10 times larger than in DEM-P-based ones.

Contact recovery speed (CRS) is a parameter used only in DEM-C-based simulations. As its name indicates, it is a parameter that puts the upped limit on the normal component of the velocity two colliding bodies rebound off each other with. In complementarity approach the bodies are modeled as they were rigid. Even though, at the beginning of each time step bodies can overlap, assigning the penetration depth to such contact. In each time step, the normal component of the velocity two bodies will rebound off each other is equal to the penetration depth divided by the time step. If the value of this component exceeds the value of the upper limit (called contact recovery speed) it is simply clamped to the value of this limit. In other words, CRS provides stability to the simulations and allows having larger values of Δt and at the same time smaller amount of maximum number of iterations per time step (MNoI). Thus, it also makes the execution time of the simulations shorter.

MNoI sets the maximum number of iterations that are done during each time step to calculate the values of the normal and tangential components of forces related to every contact.

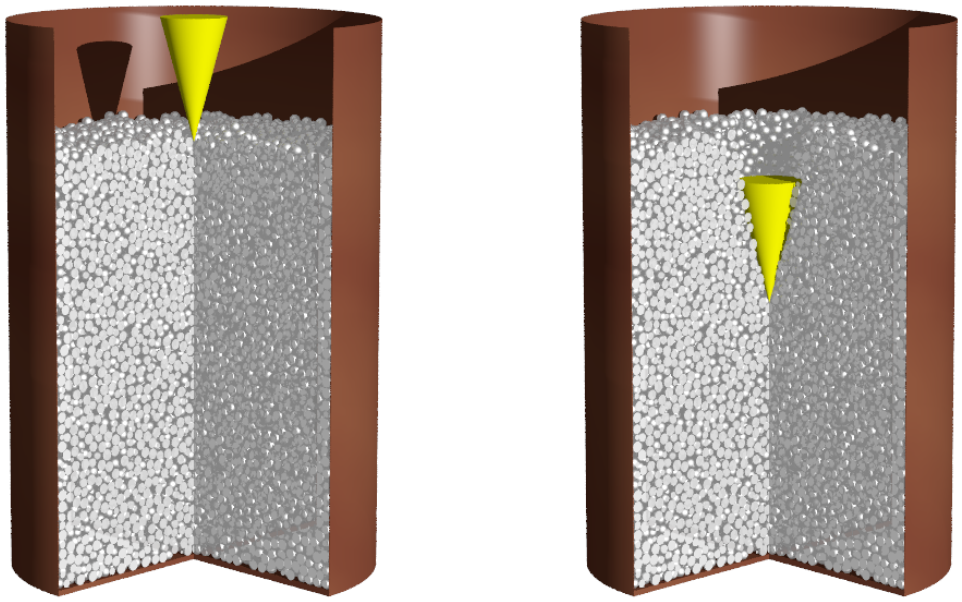

(a) (b)

Figure 13: Cone penetration test - numerical setup: (a) cone placed over the settled specimen; (b) cone penetrating the granular material.

The value of this parameter depends on the type of the simulations. In the simulation of cone penetration test (CPT) 50 iterations per time step were enough to have reasonable results. Calculations with MNoI set up to 600 gave the satisfactory results concerning shear test [7]. The simulations of standard triaxial test required the value of MNoI to be set to 2500, to have calculation that were not only stable but also giving results correct from the physical point of view [8]. The values of the above-described parameters used in the simulations of cone penetration test were presented in Table 8.

2.3 Results

In this section the results obtained from the simulations were presented and compared to the experimental data. The densities and void ratios of the samples in their equilibrium state were summarized in the Tables from 9 to 12. The relative error between the simulations and empirical test varied from 1.19 % to 5.20 % concerning densities and from 3.85 % to 13.79 % when it comes to the void ratios. The displacements of the cones as functions of time were plotted in the Figures from 14 to 21. The numerical results matched the experimental ones. Moreover, the outcomes from simulations based on DEM-P and DEM-C were comparable. It is noteworthy, taking into account the fact that those approaches model frictional contact differently and use different sets of parameters to describe physical phenomena.

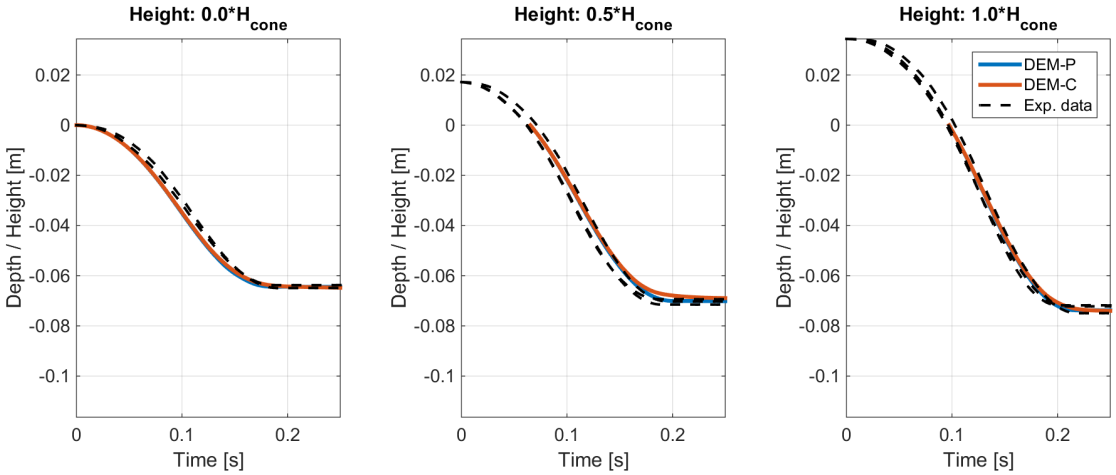

Figure 14: Hight/depth vs. time plots of the cone **30**° in apex angle. Container with a **4-inches**-wide diameter. Granular material packed **loosely**.

Densities $\left[\frac{\text{kg}}{\text{m}^3}\right]$	Experiment	Simulation		Relative Error [%]	
		DEM-P	DEM-C	DEM-P	DEM-C
Loose Case	1504.29	1449.59	1426.00	3.64	5.20
Dense Case	1630.34	1608.79	1593.69	1.32	2.25

Table 9: A comparison of the experimental and numerical results. **Densities** of the samples in their equilibrium state. Container with a diameter of **4 inches**.

Densities $\left[\frac{\text{kg}}{\text{m}^3}\right]$	Experiment	Simulation		Relative Error [%]	
		DEM-P	DEM-C	DEM-P	DEM-C
Loose Case	1504.32	1462.70	1433.39	2.77	4.72
Dense Case	1630.35	1610.93	1601.22	1.19	1.79

Table 10: A comparison of the experimental and numerical results. **Densities** of the samples in their equilibrium state. Container with a diameter of **6 inches**.

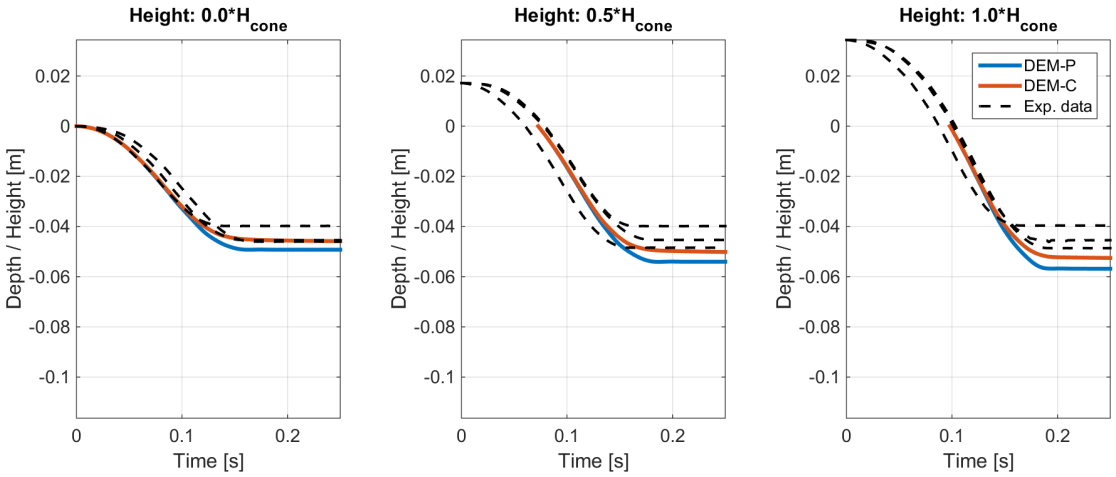

Figure 15: Hight/depth vs. time plots of the cone **30**° in apex angle. Container with a **4-inches**-wide diameter. Granular material packed **densely**.

Void Ratios	Experiment	Simulation		Relative Error [%]	
		DEM-P	DEM-C	DEM-P	DEM-C
Loose Case	0.66	0.72	0.75	9.50	13.79
Dense Case	0.53	0.55	0.57	3.85	6.61

Table 11: A comparison of the experimental and numerical results. **Void ratios** of the samples in their equilibrium state. Container with a diameter of **4 inches**.

Void Ratios	Experiment	Simulation		Relative Error [%]	
		DEM-P	DEM-C	DEM-P	DEM-C
Loose Case	0.66	0.71	0.74	7.15	12.43
Dense Case	0.53	0.55	0.56	3.46	5.23

Table 12: A comparison of the experimental and numerical results. **Void ratios** of the samples in their equilibrium state. Container with a diameter of **6 inches**.

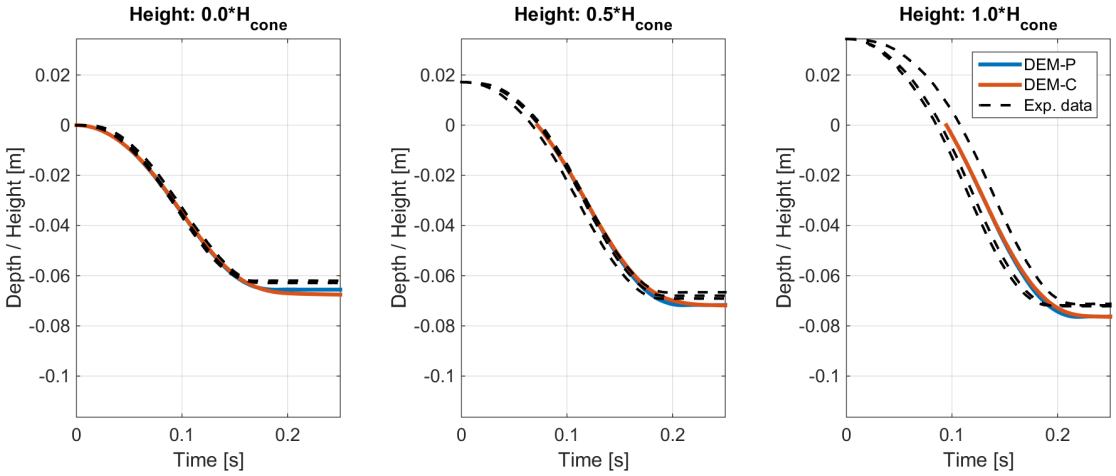

Figure 16: Hight/depth vs. time plots of the cone **30**° in apex angle. Container with a **6-inches**-wide diameter. Granular material packed **loosely**.

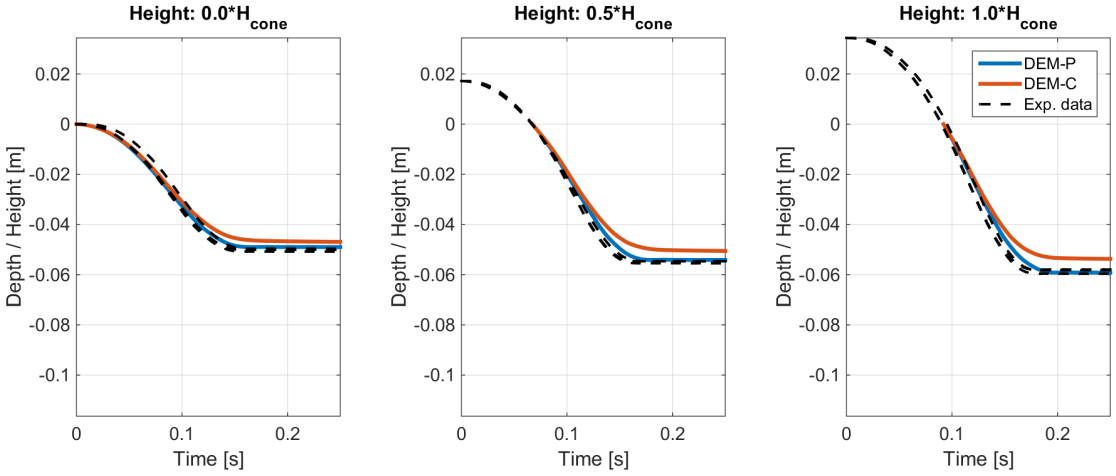

Figure 17: Hight/depth vs. time plots of the cone **30**° in apex angle. Container with a **6-inches**-wide diameter. Granular material packed **densely**.

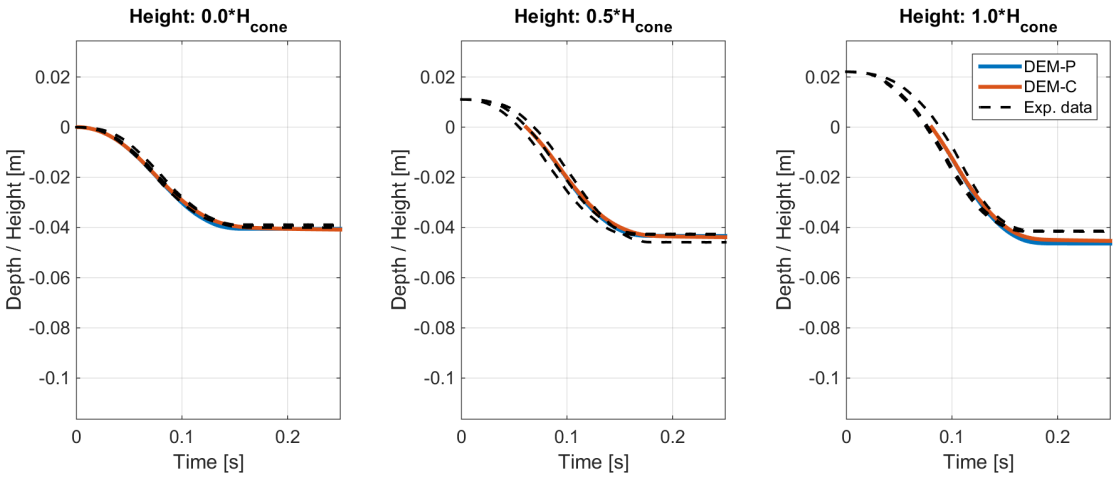

Figure 18: Hight/depth vs. time plots of the cone **60**° in apex angle. Container with a **4-inches**-wide diameter. Granular material packed **loosely**.

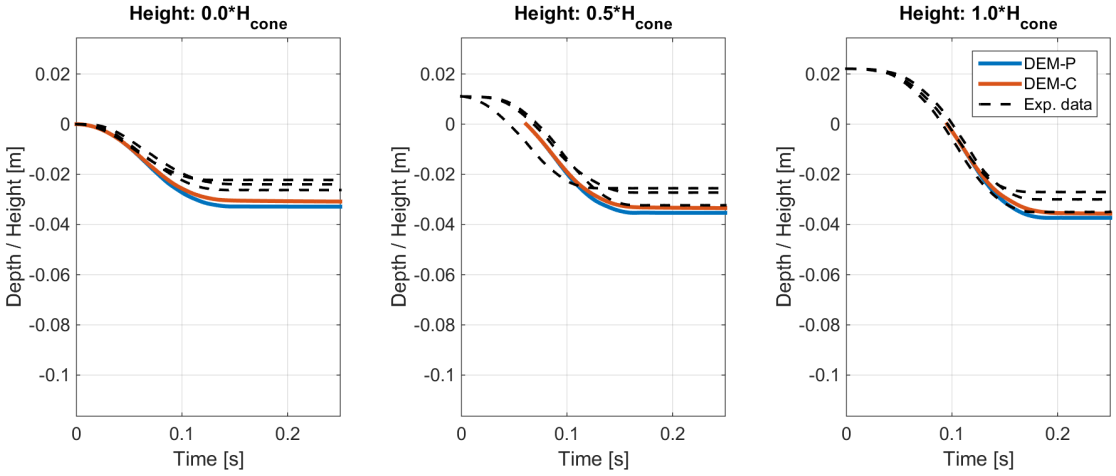

Figure 19: Hight/depth vs. time plots of the cone **60**° in apex angle. Container with a **4-inches**-wide diameter. Granular material packed **densely**.

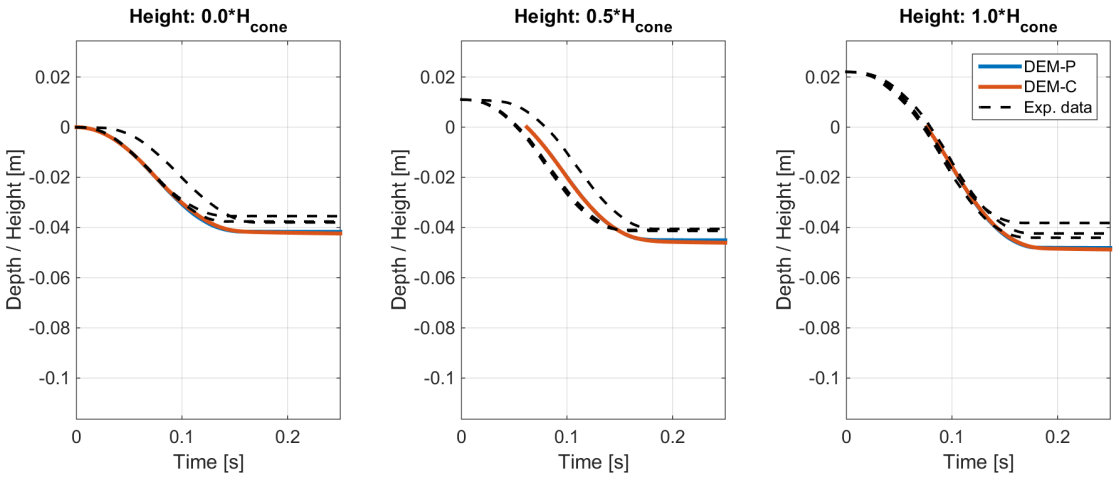

Figure 20: Hight/depth vs. time plots of the cone **60**° in apex angle. Container with a **6-inches**-wide diameter. Granular material packed **loosely**.

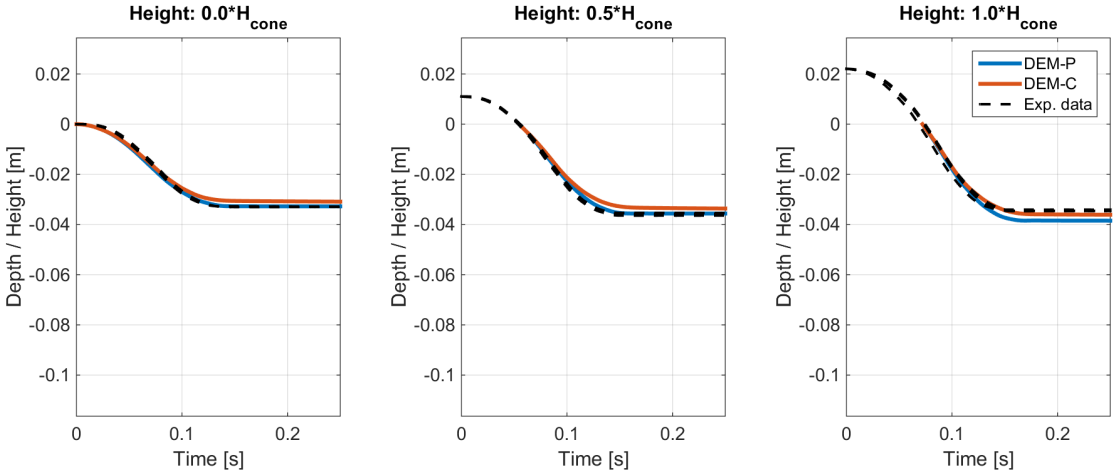

Figure 21: Hight/depth vs. time plots of the cone **60**° in apex angle. Container with a **6-inches**-wide diameter. Granular material packed **densely**.

2.4 Performance analysis

The execution time of the cone penetration simulation was discussed in this section. As mentioned previously, the simulations consisted of the two stages - settling and cone penetration stage. In the former the granular material wa poured into the container and was allowed to gain its equilibrium. The execution time of the settling stage that last 1.0 second of simulation time was presented in this section. The equilibrium was gained earlier (around 0.5 of the second; see Figure 12). In the cone penetration stage the cone was placed right at the level of the specimen's surface and dropped with the initial velocity. This stage took 0.4 seconds of the simulation time.

The performance of the simulations based on penalty and complementarity approaches was compared, resulting in the execution times of simulations based on DEM-C being about 1.6 times longer. All the simulations were run using 8 threads of Intel ES-2650 v3 @ 2.30 Ghz. Results were summarized in the Tables from 13 to 16.

Settling Stage	Execution Time (T_{exec})	Simulation time [s]	$T_{exec}^{DEM-C}/T_{exec}^{DEM-P}$
DEM-P	3 h 14 min	1.0	1.54
DEM-C	5 h 03 min		

Penetrometer Stage	Execution Time (T_{exec})	Simulation time [s]	$T_{exec}^{DEM-C}/T_{exec}^{DEM-P}$
DEM-P	1 h 21 min	0.4	1.64
DEM-C	2 h 13 min		

Whole simulation	Execution Time (T_{exec})	Simulation time [s]	$T_{exec}^{DEM-C}/T_{exec}^{DEM-P}$
DEM-P	4 h 36 min	1.4	1.56
DEM-C	7 h 16 min		

Table 13: Comparison of the execution time. Container 4-in-wide. Loose packing. Number of bodies **48864**.

Settling Stage	Execution Time (T_{exec})	Simulation time [s]	$T_{exec}^{DEM-C}/T_{exec}^{DEM-P}$
DEM-P DEM-C	3 h 33 min 5 h 55 min	1.0	1.67

Penetrometer Stage	Execution Time (T_{exec})	Simulation time [s]	$T_{exec}^{DEM-C}/T_{exec}^{DEM-P}$
DEM-P DEM-C	1 h 27 min 2 h 32 min	0.4	1.76

Whole simulation	Execution Time (T_{exec})	Simulation time [s]	$T_{exec}^{DEM-C}/T_{exec}^{DEM-P}$
DEM-P DEM-C	5 h 00 min 8 h 27 min	1.4	1.69

Table 14: Comparison of the execution time. Container 4-in-wide. Dense packing. Number of bodies **53296**.

Settling Stage	Execution Time (T_{exec})	Simulation time [s]	$T_{exec}^{DEM-C}/T_{exec}^{DEM-P}$
DEM-P DEM-C	7 h 06 min 10 h 23 min	1.0	1.46

Penetrometer Stage	Execution Time (T_{exec})	Simulation time [s]	$T_{exec}^{DEM-C}/T_{exec}^{DEM-P}$
DEM-P DEM-C	4 h 12 min 7 h 29 min	0.4	1.78

Whole simulation	Execution Time (T_{exec})	Simulation time [s]	$T_{exec}^{DEM-C}/T_{exec}^{DEM-P}$
DEM-P DEM-C	11 h 18 min 17 h 52 min	1.4	1.58

Table 15: Comparison of the execution time. Container 6-in-wide. Loose packing. Number of bodies **110786**.

Settling Stage	Execution Time (T_{exec})	Simulation time [s]	$T_{exec}^{DEM-C}/T_{exec}^{DEM-P}$
DEM-P DEM-C	7 h 28 min 10 h 47 min	1.0	1.44

Penetrometer Stage	Execution Time (T_{exec})	Simulation time [s]	$T_{exec}^{DEM-C}/T_{exec}^{DEM-P}$
DEM-P DEM-C	4 h 42 min 8 h 02 min	0.4	1.71

Whole simulation	Execution Time (T_{exec})	Simulation time [s]	$T_{exec}^{DEM-C}/T_{exec}^{DEM-P}$
DEM-P DEM-C	12 h 10 min 18 h 49 min	1.4	1.55

Table 16: Comparison of the execution time. Container 6-in-wide. Dense packing. Number of bodies **120860**.

3 Additional Analyses

3.1 Impact of the $\mu_{\text{particle-particle}}$ on the results

The impact of the inter-sphere coefficient of friction ($\mu_{\text{p-p}}$) on the depth at which the cone was stopped was discussed in this section. As expected, the larger the value of μ_{p-p} was, the earlier the cone was stopped. It is worthy to mention that the analysis of the impact of the $\mu_{\text{p-c}}$ (friction coefficient between particles and cone) had very little impact on the numerical results (see section 3.2).

To understand how sensitive the simulation is to the value of $\mu_{\text{p-p}}$, the cone penetration test (the second stage) was run for a couple of different values of this parameter. Namely, $\mu_{\text{p-p}} \in \{0.4,\ 0.5,\ 0.6,\ 0.7\}$. In every simulation the fiction coefficient between the cone and particles ($\mu_{\text{p-c}}$) was set to 0.7. The values of other numerical and mechanical parameters can be found in Tables from 5 to 7.

Due to making the plots readable (without many lines lying one next to another) curves related to $\mu_{\text{p-p}} = 0.5$ and $\mu_{\text{p-p}} = 0.7$ only were presented in the plots on Figures from 22 to 26. The trend that for larger values of $\mu_{\text{p-p}}$ the cone penetrates lesser the sample was seen on the plots. Thus, the curve corresponding to $\mu_{\text{p-p}}$ 0.6 was located between those presented on plots below. Cone's displacement related to $\mu_{\text{p-p}} = 0.4$ was located beneath all the curves (it can be also found in the section 3.2 where plots with $\mu_{\text{p-p}} = 0.4$ were showed).

Another worthy of note observation is that the difference between the curves obtained for different values of $\mu_{\text{p-p}}$ is larger in case of simulations with granular material packed loosely. On the other hand, the simulations with granular material packed densely were not very sensitive for the different values of the parameter.

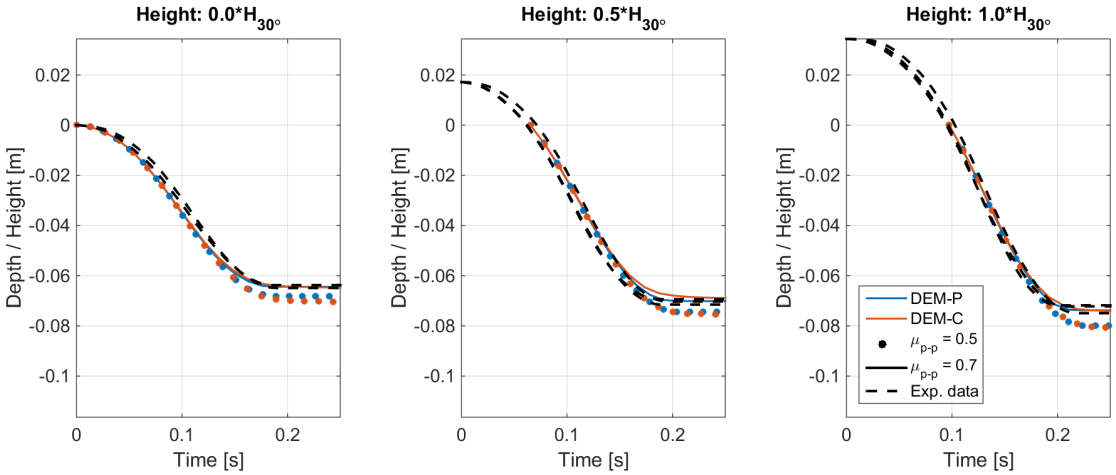

Figure 22: Hight/depth vs. time plots of the cone **30**° in apex angle. Container with a **4-inches**-wide diameter. Granular material packed **loosely**.

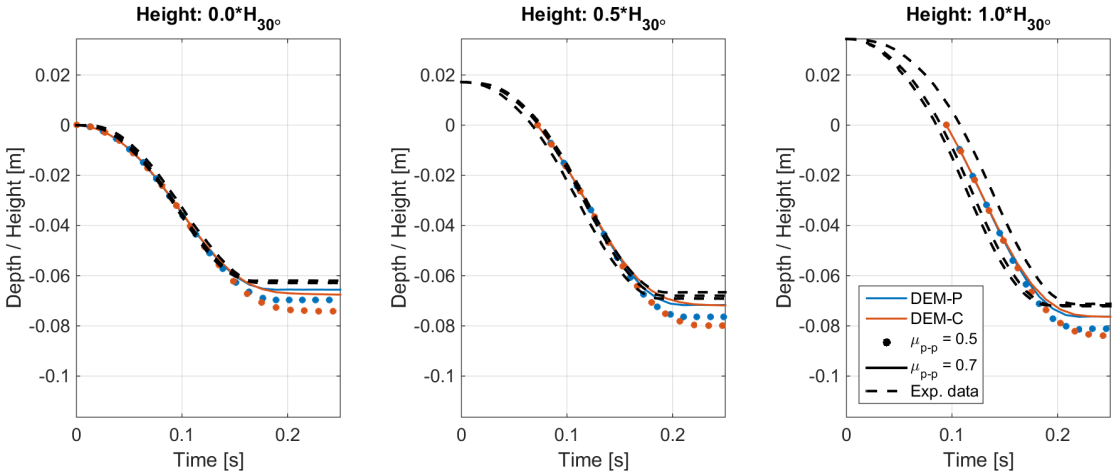

Figure 23: Hight/depth vs. time plots of the cone **30**° in apex angle. Container with a **6-inches**-wide diameter. Granular material packed **loosely**.

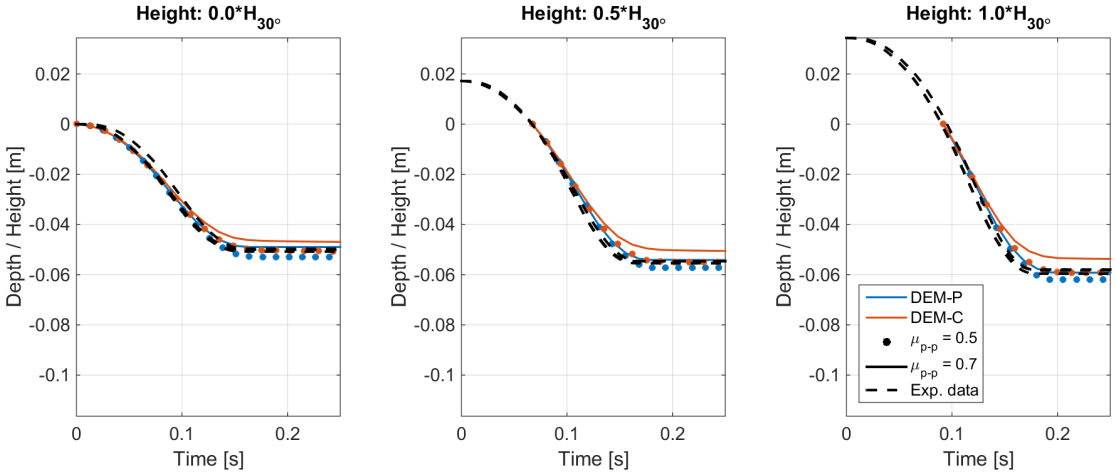

Figure 24: Hight/depth vs. time plots of the cone **30**° in apex angle. Container with a **6-inches**-wide diameter. Granular material packed **densely**.

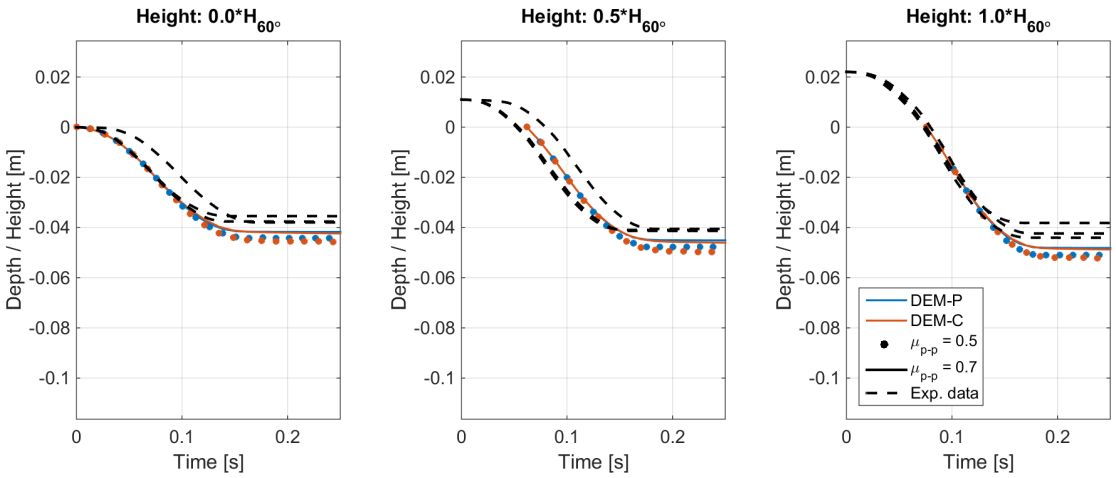

Figure 25: Hight/depth vs. time plots of the cone **60**° in apex angle. Container with a **6-inches**-wide diameter. Granular material packed **loosely**.

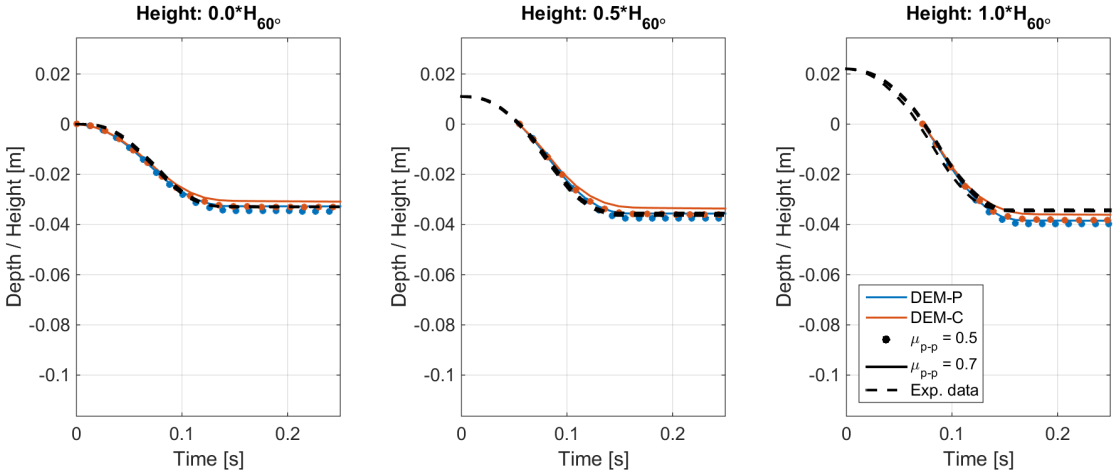

Figure 26: Hight/depth vs. time plots of the cone **60**° in apex angle. Container with a **6-inches**-wide diameter. Granular material packed **densely**.

3.2 Impact of the $\mu_{\text{particle-cone}}$ on the results

The analysis of the coefficient of friction between the granular matter and the cone ($\mu_{\text{p-c}}$) impact on the cones displacement was the objective of this section. The trend seen in section 3.1 (that the larger value of the coefficient of friction causes lesser penetration depths) was expected. It turned out that the value of this parameter influenced the results to a very little extend.

The cone penetration stage was run for $\mu_{\text{p-c}} \in \{0.5,\ 0.6,\ 0.7\}$, while the inter-particle coefficient of friction was equal to 0.4 in every simulation. The values of the rest mechanical and numerical parameters can be found in the Tables from 5 to 7. In the Figures from 27 to 31 the displacements of the cones were shown.

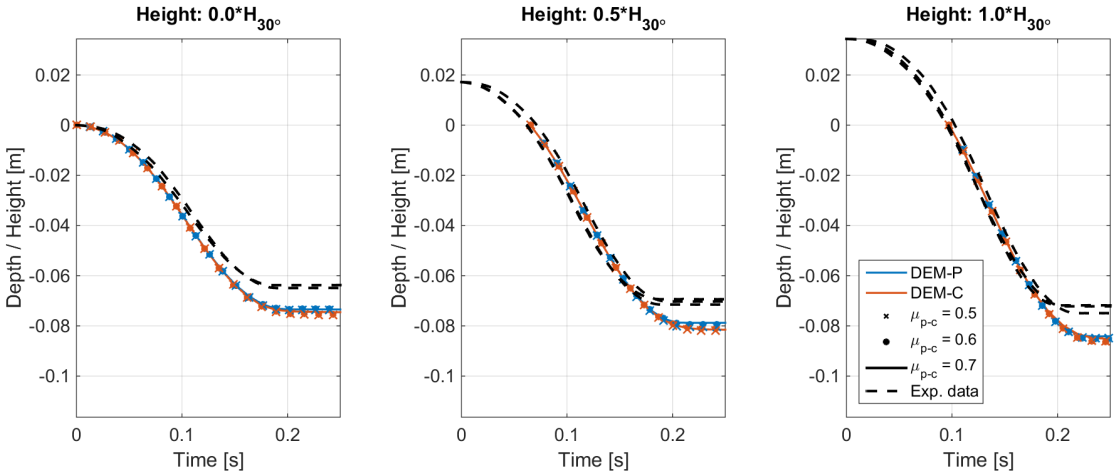

Figure 27: Hight/depth vs. time plots of the cone **30**° in apex angle. Container with a **4-inches**-wide diameter. Granular material packed **loosely**.

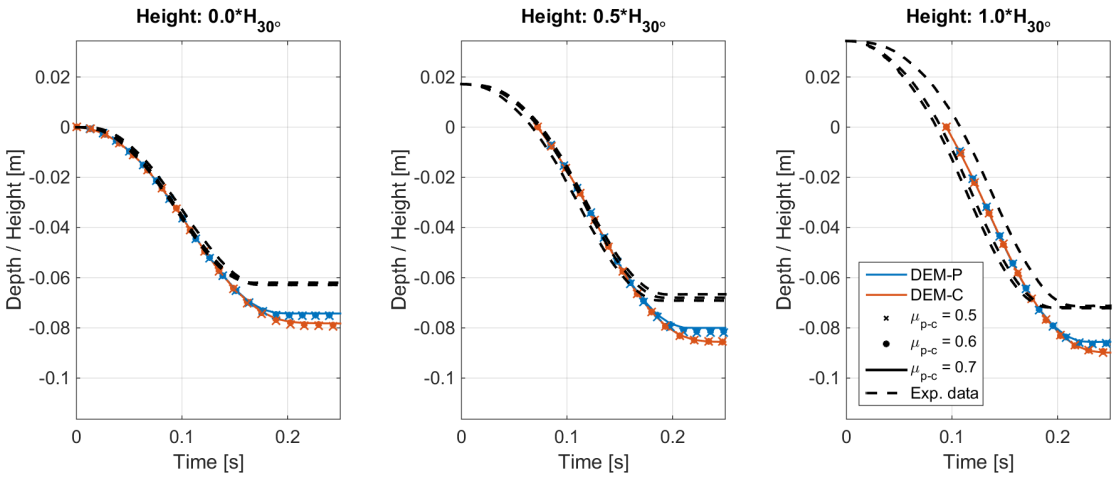

Figure 28: Hight/depth vs. time plots of the cone **30**° in apex angle. Container with a **6-inches**-wide diameter. Granular material packed **loosely**.

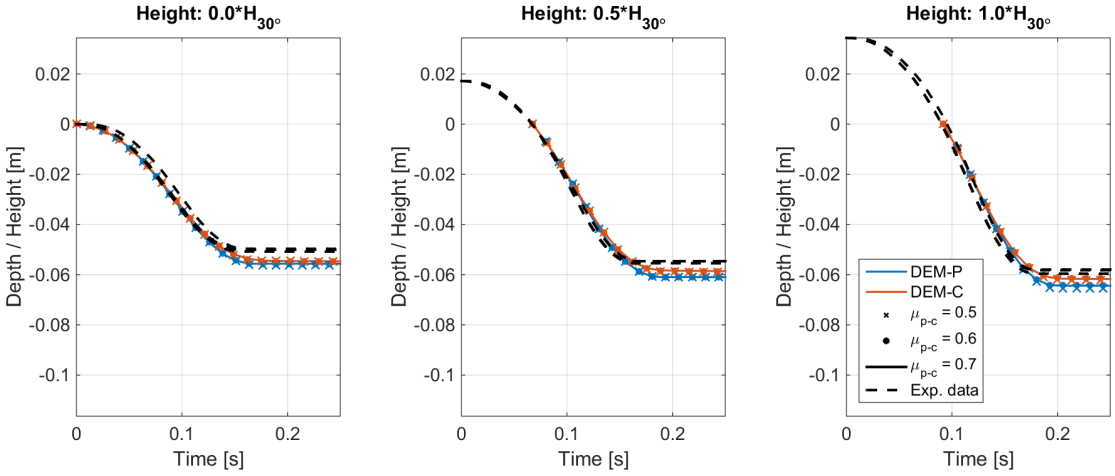

Figure 29: Hight/depth vs. time plots of the cone **30**° in apex angle. Container with a **6-inches**-wide diameter. Granular material packed **densely**.

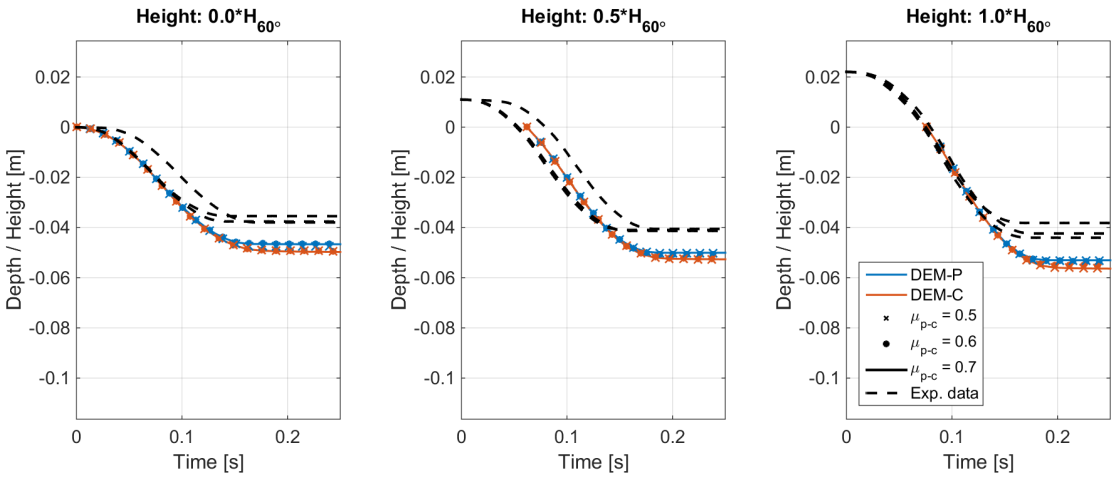

Figure 30: Hight/depth vs. time plots of the cone **60**° in apex angle. Container with a **6-inches**-wide diameter. Granular material packed **loosely**.

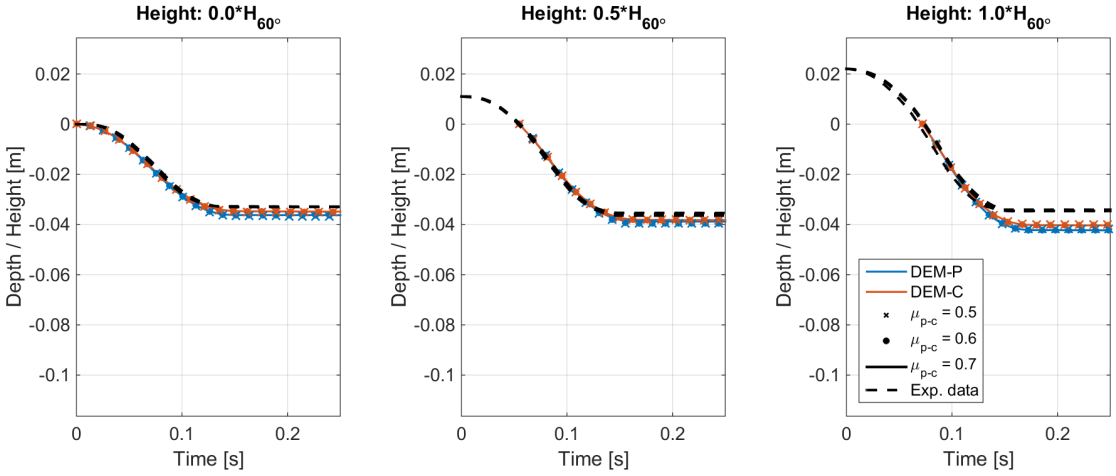

Figure 31: Hight/depth vs. time plots of the cone **60**° in apex angle. Container with a **6-inches**-wide diameter. Granular material packed **densely**.

3.3 Granular material made of the "double-spheres". The sensitivity analysis of the longitudinal dimension

The response of the mechanical system for the case where the granular material particles had a shape of "double sphere" was also investigated. A double-sphere is defined as a body that consists of two spheres of equal diameters connected to each other. Its longitudinal dimension L is equal to md, where

m is a constant real number from the range $[1.0,\ 2.0]$ and

d is a diameter of one of the spheres.

A cross-section of a double sphere with its dimensions was shown in the Figure 32. A couple of examples of such particles for different values of m were shown in the Fig. 33.

Volume (V), radii of gyration ($k_{xx},\ k_{yy},\ k_{zz}$) and principal moments of inertia ($I_{xx},\ I_{yy},\ I_{zz}$) of double sphere can be calculated from following equations:

$$V = \begin{cases} \frac{4\pi}{3}R^3(1-\cos\vartheta^*) & \text{if } \vartheta^* \in [0,\ 90^\circ] \\ \frac{4\pi}{3}R^3(1+\cos\vartheta^*) & \text{if } \vartheta^* \in [90^\circ,\ 180^*] \end{cases}$$

$$i_{xx} = i_{zz} = 2\varrho \begin{cases} \frac{2\pi}{5}R^5(1-\cos\vartheta^*) - \frac{\pi}{5}R^5\left[\frac{1}{3}(\cos^3\vartheta^* - 1) + (1-\cos\vartheta^*)\right] & \\ \quad + \frac{2\pi}{3}(z')^2R^3(1-\cos\vartheta^*) + \frac{\pi}{2}R^4(z')\sqrt{1-\cos^2\vartheta^*} & \text{if } \vartheta^* \in [0, 90^\circ] \\ \frac{2\pi}{5}R^5(1+\cos\vartheta^*) - \frac{\pi}{5}R^5\left[\frac{1}{3}(-\cos^3\vartheta^* - 1) + (1+\cos\vartheta^*)\right] & \\ \quad + \frac{2\pi}{3}(z')^2R^3(1+\cos\vartheta^*) + \frac{\pi}{2}R^4(z')\sqrt{1-\cos^2\vartheta^*} & \text{if } \vartheta^* \in [90^\circ,\ 180^\circ] \end{cases}$$

$$i_{yy} = \begin{cases} \frac{4\pi}{5}\varrho R^5\left[\frac{1}{3}(+\cos^3\vartheta^* - 1) + (1-\cos\vartheta^*)\right] & \text{if } \vartheta^* \in [0,\ 90^\circ] \\ \frac{4\pi}{5}\varrho R^5\left[\frac{1}{3}(-\cos^3\vartheta^* - 1) + (1+\cos\vartheta^*)\right] & \text{if } \vartheta^* \in [90^\circ,\ 180^\circ] \end{cases}$$

$$k_{xx}^2 = k_{zz}^2 = \frac{i_{xx}}{m} = \frac{i_{xx}}{V\varrho} \qquad k_{yy}^2 = \frac{i_{yy}}{m} = \frac{i_{yy}}{V\varrho}$$

$$I_{xx} = I_{zz} = mk_{xx}^2 \qquad I_{yy} = mk_{yy}^2$$

where:

V volume of double sphere

R radius of double sphere

z' is equal to $R - \frac{\delta}{2}$

δ is the size of the overlap between two spheres

$\cos\vartheta^*$ is equal to $\frac{z'}{R}$

ϱ density

m mass

The y-direction was parallel to the longitudinal axis of the double sphere. Two remaining directions ($x,\ z$) were (obviously) perpendicular to y-axis. Results corresponding to $\vartheta^* \in [90°,\ 180°]$ are the ones describing double sphere (L = md > d). For the case where (L = md < d) the shape of the particle starts being similar to the lens; geometrical parameters of a lens can be obtained from the formulas corresponding to $\vartheta^* \in [0, 90°]$. Differences between the equations describing lenses and double spheres were marked in red.

The sensitivity analysis of the longitudinal dimension impact on the depth at which the cone stopped penetrating the specimen was conducted on. The outcome of this analysis is showed in the Fig. 35.

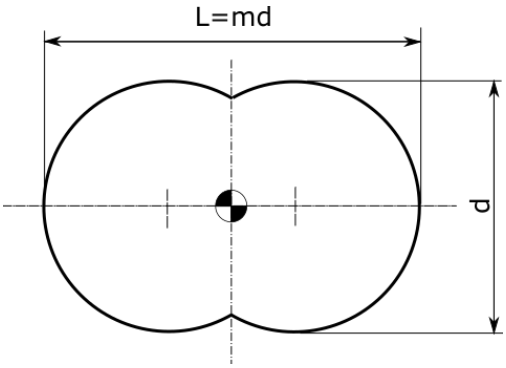

Figure 32: Dimensions of a double sphere. m $\in [1.0,\ 2.0]$

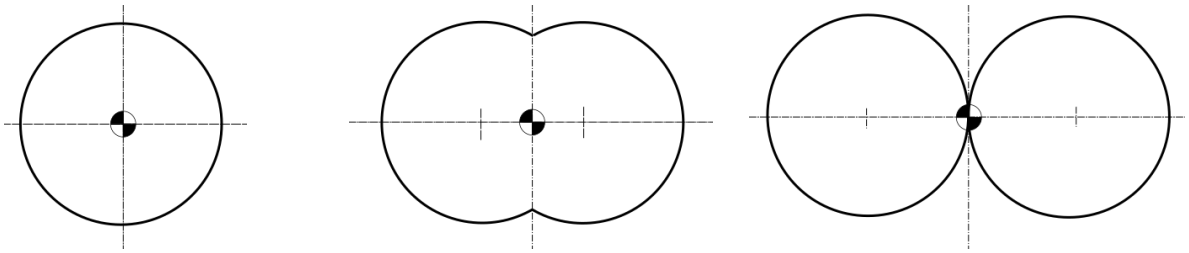

(a) m = 1.0 (b) m = 1.5 (c) m = 2.0

Figure 33: Cross-sections of double-spheres of different longitudinal dimension. In other words, double-spheres that have different values of parameter m.

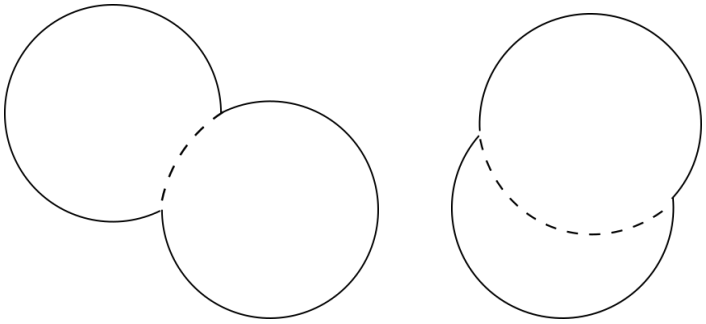

Figure 34: "Double-spheres" in 3D view

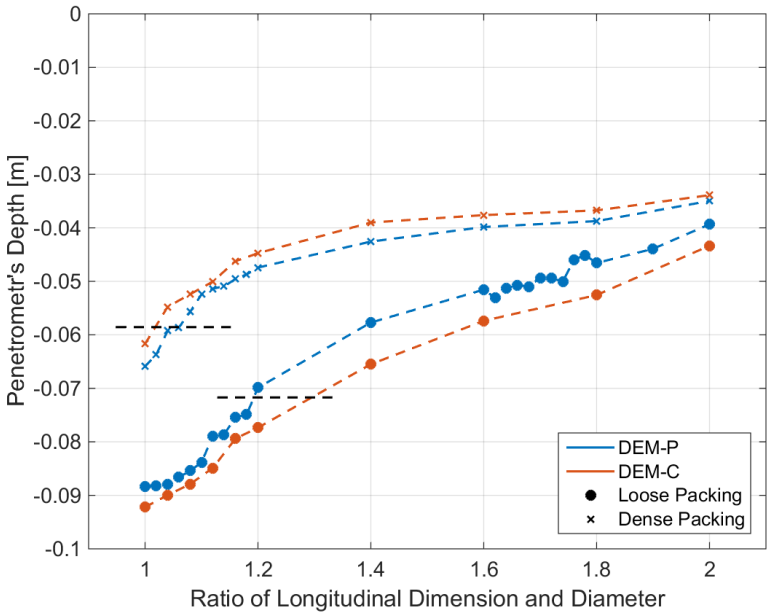

Figure 35: Depth at which the cone stopped penetrating the granular material as a function of the longitudinal dimension of the double spheres. Plot shows the results obtained from the simulations of cone having 30° in its apex angle; dropped from 34.36 mm above the specimen's surface. The granular material had the inter-particle friction coefficient equal to 0.4 and $\mu_{\text{particle-cone}} = 0.7$. Container's diameter was equal to 6 inches. Dashed lined show the depths reached by cones in the laboratory tests.

4 Conclusion

1. Results from the simulations based on DEM-P and DEM-C approaches were comparable.

2. If calibrated correctly, both DEM-P and DEM-C can be used in simulating cone penetration test, giving the results close to the experimental ones.

3. DEM-C-based simulations were around 1.6 times slower than those based on DEM-P.

4. The simulations were sensitive to the value of the inter-particle coefficient of friction.

5. The value of the coefficient of friction between the particles and cone did not have the major impact on the depths at which the cone stopped penetrating the granular material.

6. If the grains were modeled as the double-spheres, the larger their longitudinal dimension was, the smaller the penetration depths was.

References

[1] Fleischmann, J., 2015. DEM-PM Contact Model with Multi-Step Tangential Contact Displacement History. Tech. Rep. TR-2015-06, Simulation-Based Engineering Laboratory, University of Wisconsin-Madison.

[2] Negrut, D., and Serban, R., 2016. Posing Multibody Dynamics with Friction and Contact as a Differential Algebraic Inclusion Problem. Tech. Rep. TR-2016-12: `http://sbel.wisc.edu/documents/TR-2016-12.pdf`, Simulation-Based Engineering Laboratory, University of Wisconsin-Madison.

[3] Project Chrono. Chrono: An Open Source Framework for the Physics-Based Simulation of Dynamic Systems. `http://projectchrono.org`. Accessed: 2016-03-07.

[4] Williams, K., 2016. Cone penetration results for 3mm glass beads and 20-30 Ottawa sand. Tech. Rep. TR-2016-04: `http://sbel.wisc.edu/documents/TR-2016-04.pdf`, Simulation-Based Engineering Laboratory, University of Wisconsin-Madison.

[5] Elert, G. The Physics Factbook. Coefficients of Restitution, `http://hypertextbook.com/facts/2006/restitution.shtml`.

[6] The Engineering Toolbox. Friction and Friction Coefficients, `http://www.engineeringtoolbox.com/friction-coefficients-d_778.html`.

[7] Kwarta, M., and Negrut, D., 2016. Using the Complementarity and Penalty Methods for Solving Frictional Contact Problems in Chrono: Validation for the Shear-Test with Particle Image Velocimetry. Tech. Rep. TR-2016-18: `http://sbel.wisc.edu/documents/TR-2016-18.pdf`, Simulation-Based Engineering Laboratory, University of Wisconsin-Madison.

[8] Kwarta, M., and Negrut, D., 2016. Using the Complementarity and Penalty Methods for Solving Frictional Contact Problems in Chrono: Validation for the Triaxial Test. Tech. Rep. TR-2016-17: `http://sbel.wisc.edu/documents/TR-2016-17.pdf`, Simulation-Based Engineering Laboratory, University of Wisconsin-Madison.